

## Article

# Radio-Frequency Conductivity Evaluation Method Based on Surface/Interface Scattering of Metallic Coatings

Chongxiao Guo <sup>1</sup>, Ping Wu <sup>2</sup>, Yue Liu <sup>1,\*</sup>  and Tongxiang Fan <sup>1,\*</sup>

<sup>1</sup> State Key Lab of Metal Matrix Composites, School of Materials Science and Engineering, Shanghai Jiao Tong University, Shanghai 200240, China; guo083013@sjtu.edu.cn

<sup>2</sup> Key Laboratory of Advanced Science and Technology on High Power Microwave, Xi'an 710024, China; wuping@nint.ac.cn

\* Correspondence: yliu23@sjtu.edu.cn (Y.L.); txfan@sjtu.edu.cn (T.F.)

**Abstract:** Developing non-destructive evaluation methods for the radio frequency (RF) conductivity of conductive coatings can accelerate the performance evaluation and development of wireless communication devices. By using a split-resonator cavity to compare 800 nm copper/graphite and 1000 nm copper/graphite, we found that the RF conductivity increased by 45.5% and 82.7%, respectively, from 15 GHz to 40 GHz (pure copper was  $-7.2\%$ ), indicating that the bulk materials analysis method is not suitable for coating materials. Combined with electromagnetic wave theory, we believe that the critical factor lies in the additional losses of the electromagnetic waves at the copper/graphite interface and substrate. Based on the skin depth theory, the concept of triple skin depth is proposed to calculate the power loss of copper/graphite at different frequencies, considering rough  $P_{eff}$  (including the power loss of the rough surface, copper coatings, copper/graphite interface, and graphite) compared with smooth pure copper  $P_c$ . Combined with the relationship between RF conductivity and electromagnetic wave power loss, the conductivity of copper coatings  $\sigma_{Cu}$  at different frequencies is obtained by analyzing the measured  $\sigma_{eff}$ . Compared with the roughness model, the calculation error decreased from 30% to below 7%. Our study provides a theoretical basis for the regulation of the RF conductivity of metal coatings at different frequencies.

**Keywords:** copper coatings; radio frequency conductivity; split-resonator cavity; surface/interface scattering; power loss



**Citation:** Guo, C.; Wu, P.; Liu, Y.; Fan, T. Radio-Frequency Conductivity Evaluation Method Based on Surface/Interface Scattering of Metallic Coatings. *Coatings* **2024**, *14*, 599. <https://doi.org/10.3390/coatings14050599>

Academic Editor: Emilio Bellingeri

Received: 27 March 2024

Revised: 28 April 2024

Accepted: 8 May 2024

Published: 10 May 2024



**Copyright:** © 2024 by the authors. Licensee MDPI, Basel, Switzerland. This article is an open access article distributed under the terms and conditions of the Creative Commons Attribution (CC BY) license (<https://creativecommons.org/licenses/by/4.0/>).

## 1. Introduction

In modern technology, conductive surface coatings play a crucial role and find wide applications in various domains, such as electronic devices, optical devices, sensor technology, medical equipment, etc. [1–3]. Among these applications, the objective of designing and applying conductive surface coatings is to meet the requirements of the material conductivity, thereby laying the foundation for achieving higher performance and more reliable technological products [4,5]. Therefore, the precise determination of the conductivity of surface conductive coatings is crucial for determining whether the related fields can achieve rapid and efficient technological iterations and developments.

Accurately determining the conductivity of surface conductive coatings is valuable but challenging. Meng et al. employed a four-probe method to measure the resistivity of the conductive metal coatings produced by strong pulse light sintering inkjet printing, revealing that the resistivity varies with the sintering parameters [6]. A method relying on the frequency-dependent impedance of eddy current probe coils was proposed to determine the thickness and conductivity of coatings on metal plates [7]. Fleischer et al. characterized the surface conductivity of polyethylene terephthalate coated with nanowire (NW) coatings through time-domain terahertz (THz) reflectance measurements, demonstrating a strong correlation between the coating conductivity and THz field reflectance [8]. However, these

testing methods exhibit various limitations, such as destructive damage [9–11] and small testing areas that are influenced by contact resistance [12,13]. Furthermore, eddy current methods typically operate at lower frequencies, rendering them suitable for assessing coatings with thicknesses of several micrometers or for bulk conductors [14,15]. In contrast, terahertz methods are primarily ideal for conductive coatings with thicknesses of 100 nm or less [16,17]. Therefore, exploring a testing technique capable of non-destructively assessing the surface conductivity of coatings over large areas and a wide range of variable thicknesses becomes a key scientific challenge to facilitate efficient and high-quality research and the development of surface conductive coatings.

The resonant cavity testing method is non-destructive and consists of an adjustable measurement field and adjustable frequency testing for conductive coating [18–20]. Numerous studies have shown that, by adjusting the dimensions and coupling structures of the resonant cavity, it is possible to evaluate the conductivity of coatings with different sizes and thicknesses. Tran et al. measured the effective conductivity of copper-clad dielectric substrates with diameters ranging from 20 to 30 wavelengths using the resonant cavity method, achieving the frequency-dependent effective conductivity of the tested samples over a wide frequency range [18]. Nikaido proposed a similar measurement method for the interface conductivity of copper-clad dielectric substrates based on the dielectric rod resonator method. This method enabled the evaluation of the interface conductivity of substrates with varying thicknesses, and its sensitivity to substrate thickness was examined [21]. However, the existing resonant cavity testing studies mainly focus on the effective conductivity of composite substrates containing surface-coated metal coatings. This parameter encompasses the combined conductivity of the conductive metal coating, interface, and dielectric composite board, hindering the individual evaluation of the surface conductivity of the dielectric composite board. Drawing on the theory of high-frequency electromagnetic wave transmission and attenuation, and the inverse relationship between the wave penetration depth and operating frequency [22], employing very high frequencies (like the terahertz band) can effectively disregard the substrate influence, facilitating the accurate evaluation of the conductive coating's radio frequency conductivity on the substrate surface.

Ye employed a quasi-optical resonator operating at approximately 180 GHz to measure the conductivity of metal coatings on silicon substrates [23]. They developed a dual-layer effective conductivity model that correlates the conductivity of the coatings with the effective conductivity of a single layer by taking into account the attenuation and reflection of the electromagnetic waves propagating within the sample. The results indicated that the average conductivity of the 100 nm aluminum coating deposited on a silicon wafer was 16.6 MS/m, with a quasi-error of 6%. This study illuminates the evaluation of the radio frequency (RF) conductivity in surface coatings within dual-layer structures. However, this method relied on a quasi-optical resonator at approximately 180 GHz, limiting measurements across frequencies and coating thicknesses. In addition, Ye did not fully consider the influence of the rough coating surface interfaces and substrates on electromagnetic wave absorption, which is supposed to have a notable impact on the transmission and absorption of electromagnetic waves in dual-layer structures [24,25].

When conducting radio frequency conductivity tests on conductive coatings with varying thicknesses across different frequencies, it is crucial to consider two scenarios with a constant coating thickness. The first scenario is that the electromagnetic waves attenuate entirely within the conductive coating, and the second scenario arises when the electromagnetic waves penetrate the conductive coating but fully attenuate within the substrate [26]. According to the theory of skin depth for electromagnetic waves, the thickness of the conductive coating should be at least three times greater than the skin depth to ensure complete attenuation within the coating. Consequently, when measuring the radio frequency conductivity of conductive coatings with varying thicknesses at different frequencies, it is crucial to consider the relationship between the coating thickness and three times the skin depth corresponding to the frequency. Therefore, the RF conductivity of the

conductive coating for a specific rough surface in a dual-layer conductive structure should be evaluated based on two conditions: (a) constructing a reasonable surface model for the rough coating to depict the surface roughness and then calculating the extra power loss of the input electromagnetic wave induced by the rough surface, and (b) considering the correlation between the coating thickness and three times the skin depth associated with the test frequency to deduce the attenuation and reflection processes of the electromagnetic waves within the sample, and establishing a link between the coating's conductivity and the sample's effective conductivity [27,28].

This study employed a split resonator testing technique with adjustable frequency (15–40 GHz) to measure the conductivity of copper (Cu) coatings with different thickness values (800 nm and 1000 nm) on graphite surfaces. This method simultaneously considers both the skin depth ( $\delta_s$ ) and triple skin depth ( $3\delta_s$ ) of the Cu at the frequency range of 15–40 GHz. By adjusting the test frequency, the method accommodates varying penetration depths of electromagnetic waves, ranging from the surface Cu coatings to the graphite substrate. This facilitates the assessment of the radio frequency conductivity of the Cu coatings at different thicknesses and frequencies. The specific implementation process involves proposing a fractal model for surface roughness, computing the ratio of the power loss between the rough and smooth surfaces in the resonator at different frequencies, and deriving the radio frequency conductivity of the Cu coatings on rough surfaces when the thickness of the coatings exceeds  $3\delta_s$ . Subsequently, additional calculations are conducted to determine the power loss caused by the interface and substrate, establishing the numerical relationship between the conductivity of the coatings ( $\sigma_{Cu}$ ) and the effective conductivity of the Cu/graphite ( $\sigma_{eff}$ ). This enables the calculation of the radio frequency conductivity of the Cu coatings when the thickness is less than  $3\delta_s$ .

## 2. Experiments and Test Principles

In this experiment, we focused on the resonant mode denoted as  $TE_{mnp}$  and determined the resonant frequencies of four specific modes within the resonant cavity. By setting  $p = 1, 3, 5, 7$  and  $m = 0$  and  $n = 1$ , these modes are labeled as  $TE_{011}$ ,  $TE_{013}$ ,  $TE_{015}$ , and  $TE_{017}$ . Derived from the  $TE_{mnp}$  resonant frequency expressed in Formula (1), we identified the resonant frequencies for the four modes as 15, 21, 30, and 40 GHz, respectively [29]:

$$f_{01p} = \frac{c}{2\pi\sqrt{\mu\epsilon}} \sqrt{\left(\frac{u'_{01}}{a}\right)^2 + \left(\frac{p\pi}{2l}\right)^2} \quad (1)$$

where  $c$  is the speed of light,  $a$  stands for the radius of the cavity, with a length of  $2l$ .  $\mu$  and  $\epsilon$  represent the magnetic permeability and complex permittivity of the filling medium inside the cavity, respectively, where the filling medium is air.

The entire testing system comprises a Vector Network Analyzer (VNA, version number: ZNB40, Rohde & Schwarz Asia Pte Ltd., 9 Changi Business Park Vis, Singapore) and a cylindrical resonant cavity, connected by a high-frequency cable. The sample under test is placed at the bottom of the resonant cavity, and the coupling effect at different frequencies is adjusted by controlling the coupling loop. The VNA is operated using library functions from the GPIB software Iolibsuite (version number: Keysight IO Libraries Suite 2022), developed by Agilent Technologies (Santa Clara, CA, USA), facilitating data communication with the computer [30]. The testing software is developed using the Matlab software platform (version number: R2023a Win). The raw data obtained from Matlab software represent the Q factor of the testing system at a specific measured frequency point. The procedure of calculating the RF conductivity from the Q factor is outlined as follows [20,31–33]:

When utilizing the  $TE_{01p}$  mode as the testing configuration, the electromagnetic field within the resonant cavity can be represented by

$$H_r = H_0 \frac{Ba}{u'_{01}} J'_0 \left( \frac{u'_{01}}{a} r \right) \cos Bz \quad (2)$$

$$H_z = H_0 J_0 \left( \frac{u'_{01}}{a} r \right) \sin Bz \tag{3}$$

$$E_\varphi = jH_0 k \eta \frac{a}{u'_{01}} J'_0 \left( \frac{u'_{01}}{a} r \right) \sin Bz \tag{4}$$

where  $B = p\pi/L$ ,  $\eta = \sqrt{\mu/\epsilon}$ ,  $k = \omega\sqrt{\mu\epsilon}$ .  $\omega$  is the angular frequency,  $H_0$  is the coefficient determined from the boundary conditions,  $J'_0(x)$  is the derivative of the first kind of the Bessel function, and  $u'_{01}$  is the first root of  $J'_0(x)$ .

When the resonant cavity reaches the resonant state, the stored magnetic field energy and electric field energy in the cavity are equal. The energy storage can be calculated based on  $E_\varphi$  as follows:

$$W = 2W_e = \frac{\epsilon}{2} \int_{z=0}^L \int_{\varphi=0}^{2\pi} \int_{r=0}^a |E_\varphi|^2 r dr d\varphi dz \tag{5}$$

The resonant cavity is weakly coupled throughout the entire testing process, and, in this case, the measured loaded quality factor  $Q_u$  of the cavity can be approximated as the unloaded quality factor  $Q_c$ , provided by

$$Q_u \approx Q_c = \omega \frac{W}{P_c + P_d} \tag{6}$$

where  $P_c$  denotes the metal loss on the cavity wall, and  $P_d$  represents the dielectric loss of the filling medium within the cavity. When evaluating the surface resistivity of the metal material, the resonant cavity operates in the empty cavity state with air as the filling medium. Consequently, the dielectric loss  $P_d$  can be ignored, focusing solely on the cavity wall metal loss  $P_c$ .  $P_c$  correlates with the microwave surface resistivity of the cavity wall material at the testing frequency and the magnetic field component along the tangent direction of the cavity wall.  $P_c$  is provided by

$$P_c = \frac{R_w}{2} \oint_S |J_s|^2 ds = \frac{R_s}{2} \oint_S |H_{tan}|^2 ds \tag{7}$$

where  $J_s$  stands for the current on the cavity wall,  $H_{tan}$  represents the tangential component of the magnetic field along the cavity wall, and  $R_w$  denotes the microwave surface resistivity of the cavity wall metal material.  $P_c$  originates from three sources of loss:  $P_{c1}$  on the cylindrical surface,  $S_1$  of the side wall,  $P_{c2}$  on the upper cover plate,  $S_2$  of the resonant cavity, and  $P_{c3}$  on the lower cover plate (i.e., the tested sample flat plate  $S_3$ ).

By substituting the field expressions from Equations (2)–(6) into Equation (7), the expressions for various losses on the cavity wall can be obtained as follows:

$$P_{c1} = \frac{R_{s1}}{2} \int_{S_1} |H_z(r = a)|^2 ds \tag{8}$$

$$P_{c2} = \frac{R_{s2}}{2} \int_{S_2} |H_r(z = L)|^2 ds \tag{9}$$

$$P_{c3} = \frac{R_{s3}}{2} \int_{S_3} |H_r(z = 0)|^2 ds \tag{10}$$

where  $R_{s1}$ ,  $R_{s2}$ , and  $R_{s3}$  represent the microwave surface resistivity of surfaces  $S_1$ ,  $S_2$ , and  $S_3$ , respectively. Therefore, the loaded quality factor can be expressed as follows:

$$Q_u = \frac{\omega_0 W}{P_{c1} + P_{c2} + P_{c3}} \tag{11}$$

Subsequently,  $R_s$  can be calculated by measuring the quality factor  $Q_u$  based on the value of Equation (11). After obtaining the microwave surface resistivity  $R_s$ , the following formula can be employed to determine the corresponding high-frequency conductivity  $\sigma_{eff}$ :

$$R_s = \sqrt{\frac{\pi f \mu_0}{\sigma_{eff}}} (\Omega) \quad (12)$$

$$\sigma_{eff} = \frac{\pi f \mu_0}{R_s^2} (\text{S/m}) \quad (13)$$

where  $\mu_0 = 4\pi \times 10^{-7}$ .

The Cu coatings with different thicknesses on graphite surface were deposited by ion plating technology; the details can be seen in [34,35]. The thickness uniformity of the Cu coatings is examined using a JSM-7800F scanning electron microscope (JEOL Ltd., Tokyo, Japan) to minimize the influence of uneven coating thickness on RF conductivity results. Confocal microscopy (COM, RX-100, Hirox Co., Ltd., Tokyo, Japan) was employed to measure the height difference on the Cu/graphite. The analysis software of testing system provides relevant information about the test surface, including surface roughness ( $R_{rms}$ ) and the sampling length of the rough surface ( $L_1$ ).

### 3. Results and Discussion

The microscopic morphology of the cross-section of Cu/graphite (represented by Cu/Gr in Figure 1) was initially examined. As shown in the enlarged region of the red box in Figure 1a, the thickness of the Cu coatings is approximately  $800 \pm 50$  nm. Figure 1b indicates that the thickness of the Cu coating is approximately  $1000 \pm 50$  nm. The thickness of the Cu coatings varied slightly in different positions, mainly due to the height fluctuations of the graphite substrate. Figure 1c–e further highlights this undulation effect, which showcases the confocal 3D morphology of the pure Cu and Cu/graphite. The surface roughness values for the pure Cu, 800 nm Cu/graphite, and 1000 nm Cu/graphite were calculated as 60 nm, 432 nm, and 460 nm, respectively. These values were determined by the surface height differences measured using confocal microscopy.

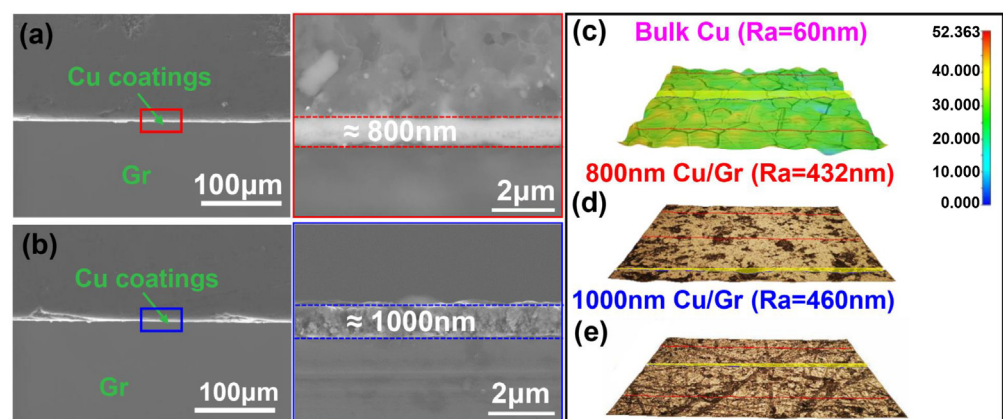


**Figure 1.** Cu/graphite cross-section morphology and surface Cu height difference distribution: (a) 800 nm Cu/graphite cross-section micro-morphology; (b) 1000 nm Cu/graphite cross-section micro-morphology; (c) Pure Cu surface height difference distribution; (d) 800 nm Cu/graphite surface height difference distribution; (e) 1000 nm Cu/graphite surface height difference distribution.

Subsequently, both the 800 nm and 1000 nm Cu/graphite were examined regarding the trends in RF conductivity with frequency (represented by Cu/Gr in Figure 2). A comparison with the trend observed for pure Cu is presented in Figure 2a. The RF conductivity of the pure Cu decreases slightly with increasing frequency, ranging from 50 MS/m to 56 MS/m. In contrast, the RF conductivity of the Cu/graphite increases

with rising frequency, as depicted in Figure 2b, c. Notably, the RF conductivity of the Cu/graphite reaches the highest value at 40 GHz, with 2.4 MS/m of 800 nm Cu/graphite and 7.3 MS/m of 1000 nm Cu/graphite. To further investigate the RF conductivity trends with frequency for the Cu/graphite and pure Cu, an assessment was conducted to compare the RF conductivity differences between the pure Cu and Cu/graphite at 15 GHz, 21 GHz, and 30 GHz with those at 40 GHz, as shown in Figure 2d. The RF conductivity of the pure Cu increases by more than 5% at 15–30 GHz, with increments of 4.0 MS/m, 3.8 MS/m, and 2.7 MS/m, respectively, compared to 40 GHz. Conversely, the RF conductivity of the 800 nm Cu/graphite decreases by 0.75 MS/m, 0.46 MS/m, and 0.28 MS/m, respectively, at 15–30 GHz compared to 40 GHz, resulting in more than a 10% decrease. Similarly, the RF conductivity of the 1000 nm Cu/graphite decreases by 3.3 MS/m, 2.3 MS/m, and 1.0 MS/m, respectively, at 15–30 GHz, exhibiting a decrease of more than 10% from the values observed at 40 GHz.

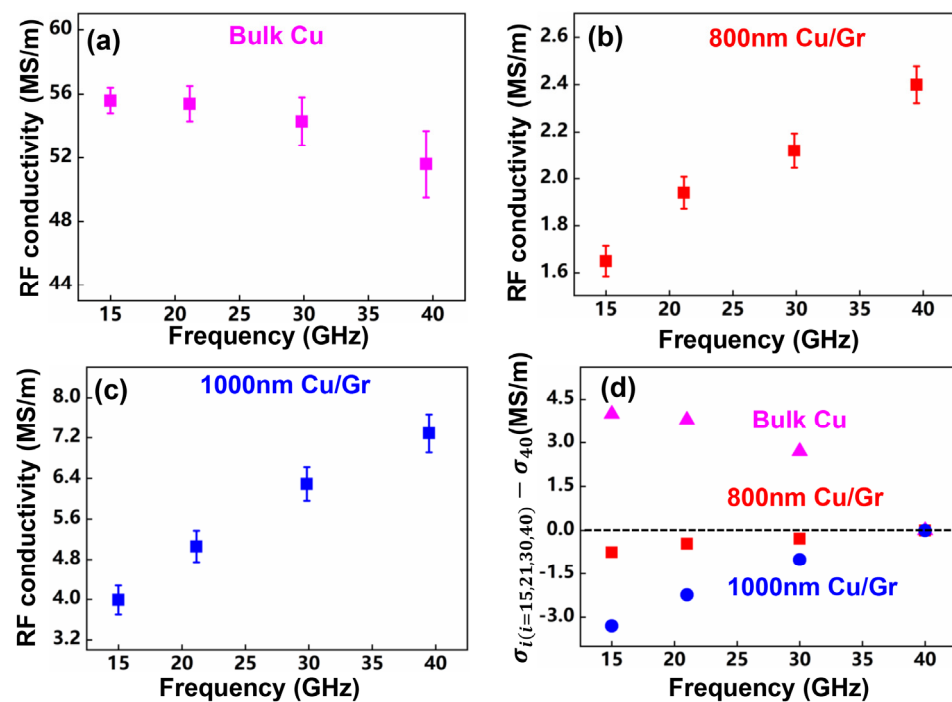


**Figure 2.** Trend of RF conductivity with frequency for pure Cu and Cu/graphite: (a) RF conductivity with frequency variation for pure Cu; (b) RF conductivity with frequency variation for 800 nm Cu/graphite; (c) RF conductivity with frequency variation for 1000 nm Cu/graphite; (d) difference in RF conductivity between pure Cu and Cu/graphite at the three frequency points of 15–30 GHz and 40 GHz.

In both the 800 nm Cu/graphite and 1000 nm Cu/graphite, the thickness of the Cu coatings adequately exceeds the skin depth of Cu at 15–40 GHz (540 nm–330 nm), supporting the assumption that electromagnetic waves decay exclusively within Cu layer [36]. Thus, the main difference between the Cu/graphite and pure Cu lies in their distinct surface roughness. According to Equations (8)–(13), the RF conductivity exhibits an inverse correlation with the microwave power loss of the material. Numerous studies have demonstrated that the additional absorption and reflection of microwaves can be non-negligible when the surface roughness exceeds a certain threshold value [37,38]. For the 800 nm Cu/graphite, the skin depth (approximately 550 nm) and surface roughness (432 nm) are comparable in magnitude at a test frequency of 15 GHz. Consequently, the influence of the surface roughness on the electromagnetic waves must be considered when calculating the conductor loss during waveguide transmission.

However, the exclusive influence of the surface roughness fails to account for the observed trend of rising RF conductivity in the Cu/graphite samples with frequency. For the pure Cu, it can be assumed that the power loss ( $P_{loss}$ ) of the electromagnetic wave transmission at four frequency points from 15 to 40 GHz is represented as  $P_{loss-15\text{GHz}}-P_{loss-40\text{GHz}}$ , with the corresponding RF conductivity denoted as  $\sigma_{15\text{GHz}}-\sigma_{40\text{GHz}}$ . The  $P_{loss}$  primarily consists of two components, as shown in Equation (14): the power loss due to surface roughness  $P_r$  and the ohmic loss  $P_C$ , arising from the conductor's inherent resistance [39]:

$$P_{loss} = P_r + P_C \quad (14)$$

With the increased frequency, the skin depth of the pure Cu ( $\delta_{Cu}$ ) gradually decreases, while the fluctuation of the rough surface remains unchanged. Consequently, the ratio of the rough surface to the skin depth gradually increases, resulting in an increased power loss of the rough surface to the electromagnetic wave, i.e.,  $P_{r-15\text{GHz}} < P_{r-40\text{GHz}}$ . Because  $P_C$  is solely related to the material itself, it can be concluded that  $P_{loss-15\text{GHz}} < P_{loss-40\text{GHz}}$  based on Formula (14). Furthermore, based on the inverse relationship between RF conductivity and microwave power loss of conductor, it can be deduced that  $\sigma_{15\text{GHz}} > \sigma_{40\text{GHz}}$ . Similarly, it can be concluded that  $\sigma_{15\text{GHz}} > \sigma_{21\text{GHz}} > \sigma_{30\text{GHz}} > \sigma_{40\text{GHz}}$ .

In view of the preceding analysis, an escalation in the surface roughness of the material contributes solely to a more evident inclination for the RF conductivity to decrease with increasing frequency. This finding has been supported by other studies as well [40]. It is worth noting that the aforementioned analysis is predicated on the material being a pure metal. Regardless of whether the skin depth decreases or increases, the skin layer remains the metal itself. In other words,  $P_C$  is only associated with the material itself and does not increase with higher frequencies. In bilayer-structured materials, such as Cu/graphite in this study, when the frequency is below 15 GHz, the skin layer includes surface Cu coatings, interfaces, and substrates. Hence, it is essential to investigate whether the skin depth contains interfaces and substrates within the 15–40 GHz range. According to the skin effect theory, the propagation factor within a material is determined when a plane wave is incident on the smooth surface of a planar metal [41]:

$$e^{-\gamma cy} = e^{-\alpha cy} \cdot e^{-j\beta cy} \quad (15)$$

The depth at which the amplitude attenuates to  $e^{-1}$  times its initial value is defined as the skin depth, denoted as  $\delta_s$ , provided by [42]

$$e^{-\alpha_c \delta_s} = e^{-1} \quad (16)$$

It is essential to note that  $\delta_s$  represents only the region where 63.2% ( $\approx 1 - e^{-1}$ ) of the current is concentrated. The region containing 95% of the current is concentrated within  $3\delta_s$ , and the region containing 98.2% of the current is concentrated within  $4\delta_s$ . Clearly, for pure metals, considering  $\delta_s$  or  $4\delta_s$  does not alter the trend of decreasing RF conductivity with increasing frequency. However, for the Cu/graphite, focusing solely on  $\delta_s$  is not realistic due to the 36.8% current conduction in the interface and substrates. Considering the significant difference in intrinsic conductivity between the substrate graphite and Cu coatings, this scenario cannot be directly compared to the case of pure metal. Essentially, it is crucial for the Cu/graphite to consider the electromagnetic wave loss within  $3\delta_s$  to assess the power loss of the material's electromagnetic field with varying frequency at least. As a result, despite the thickness of the Cu coatings being higher than the  $\delta_s$ , it is not valid to assume that the electromagnetic wave only attenuates within the Cu coatings. The RF conductivity of the Cu/graphite shown in Figure 2 actually corresponds to the effective conductivity, which encompasses the rough Cu coatings, the Cu/graphite interface, and the graphite substrate.

Based on the analysis above, the skin depth of Cu/graphite includes rough Cu film, Cu/graphite interface, and graphite substrate. To distinguish it from pure Cu, it can be

assumed that the power loss ( $P'_{loss}$ ) of electromagnetic wave transmission from 15 to 40 GHz is represented as  $P'_{loss-15GHz} - P'_{loss-40GHz}$ , and the corresponding RF conductivity is denoted as  $\sigma'_{15GHz} - \sigma'_{40GHz}$ . The  $P'_{loss}$  primarily consists of four aspects: the power loss due to surface roughness  $P'_r$ , the ohmic loss  $P'_C$  arising from the conductor's inherent resistance, the power loss  $P_i$  due to Cu/graphite interface, and power loss  $P_{substrate}$  from graphite substrate. As the frequency increases, although the power loss of the rough surface gradually increases, the power loss caused by the graphite is significantly reduced due to the reduction in the thickness of the graphite substrate in the skin depth. Since the conductivity of graphite is three orders of magnitude lower than that of Cu, the reduction in power loss of graphite with the increased frequency is significantly lower than that increasing power loss by the rough surface. Therefore, it can be concluded that  $P'_{loss-15GHz} > P'_{loss-40GHz}$ . Similarly, it can be deduced that  $\sigma'_{15GHz} < \sigma'_{21GHz} < \sigma'_{30GHz} < \sigma'_{40GHz}$ , which is consistent with the trend shown in Figure 2d.

According to the skin effect theory, the attenuation of electromagnetic waves in Cu/graphite should consider the relationship between the thickness of Cu coatings and  $3\delta_{Cu}$ . Figure 3 depicts the relationship between electromagnetic wave power loss and effective conductivity for the 800 nm Cu/graphite and 1000 nm Cu/graphite at frequencies ranging from 15 to 40 GHz, taking the  $3\delta_{Cu}$  condition into account. When the skin depth of Cu ( $\delta_{Cu}$ ) falls within 250 nm–650 nm and the thickness of Cu coatings ( $d_{Cu}$ ) is 600–1200 nm, it can be segmented into two regions labeled as  $d_{Cu} \geq 3\delta_{Cu}$  and  $d_{Cu} < 3\delta_{Cu}$  to elucidate the numerical relationship between  $d_{Cu}$  and  $3\delta_{Cu}$ , highlighted by the light red and light blue areas in Figure 3a. For a Cu thickness of 1000 nm, it falls within the  $d_{Cu} \geq 3\delta_{Cu}$  region when the test frequency is 40 GHz. Moreover, all other testing conditions fall within the  $d_{Cu} < 3\delta_{Cu}$  region.

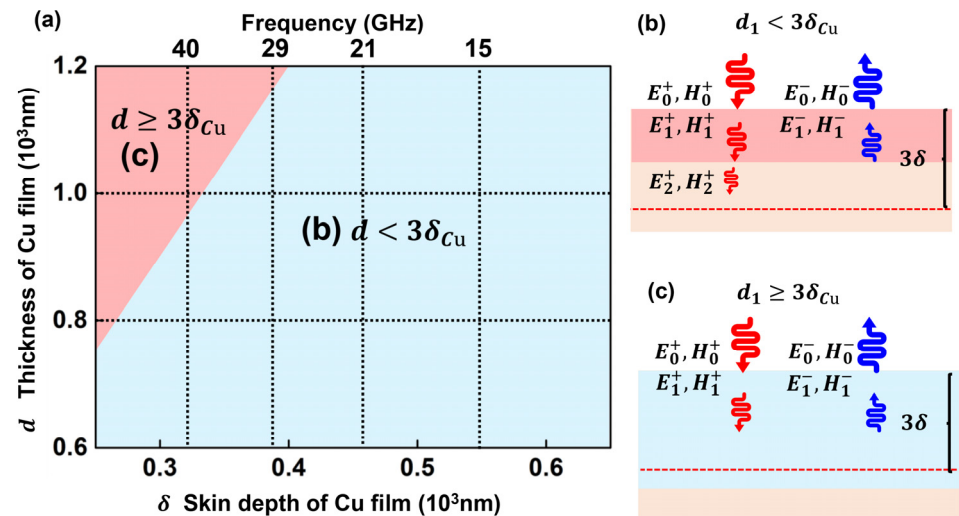


**Figure 3.** The numerical relationship between the Cu thickness of Cu/graphite and the values of  $3\delta_{Cu}$  at test frequencies of 15–40 GHz, as well as the corresponding relationship between electromagnetic wave attenuation, power loss, and effective conductivity: (a) the numerical relationship between the Cu thickness of Cu/graphite and the values of  $3\delta_{Cu}$  at test frequencies of 15–40 GHz; (b) the relationship between electromagnetic wave attenuation, power loss, and effective conductivity when  $d_{Cu} < 3\delta_{Cu}$ ; (c) the relationship between electromagnetic wave attenuation, power loss, and effective conductivity when  $d_{Cu} \geq 3\delta_{Cu}$ .

On the basis of the above analyses, the relationship between electromagnetic wave power loss and effective conductivity for the 800 nm Cu/graphite and 1000 nm Cu/graphite at frequency points from 15 to 40 GHz is classified into two cases, illustrated in Figure 3b,c. When  $d_{Cu} < 3\delta_{Cu}$ , electromagnetic waves are incident vertically on the Cu surface from air and undergo reflection and transmission phenomena at the interface, as elucidated by electromagnetic wave transmission theory. This superposition of incident and reflected waves

within Cu coatings results in a specific level of attenuation. The electromagnetic waves then propagate through graphite until complete attenuation, as illustrated in Figure 3b. The attenuation process of electromagnetic waves in Cu/graphite can be characterized by the reflection coefficient [43], denoted as  $\Gamma$ . According to Ye and Bai’s study, the total reflection coefficient of the bilayer structure can be calculated as follows:

According to the boundary conditions at the interface of “air/Cu coatings”,

$$\begin{cases} E_0^+ + E_0^- = E_1^+ + E_1^- \\ H_0^+ + H_0^- = H_1^+ + H_1^- \end{cases} \quad (17)$$

Similarly, at the interface of the “Cu/graphite substrate”,

$$\begin{cases} E_1^+ \exp(-\gamma_m d_{Cu}) + E_1^- \exp(\gamma_m d_{Cu}) = E_2^+ \exp(-\gamma_s d_{Cu}) \\ H_1^+ \exp(-\gamma_m d_{Cu}) + H_1^- \exp(\gamma_m d_{Cu}) = H_2^+ \exp(-\gamma_s d_{Cu}) \end{cases} \quad (18)$$

where  $\gamma_m$  is propagation constant in the thin film,

$$\gamma_m = (1 + j) / \delta_m \quad (19)$$

here,  $\delta_m$  is the skin depth in Cu coatings

$$\delta_m = \frac{1}{\sqrt{\pi f \mu_0 \sigma_{Cu}}} \quad (20)$$

$j$  is imaginary unit, and  $\mu_0$  is the permeability of the vacuum. Similarly, the propagation constant in substrate is

$$\gamma_s = j2\pi f \sqrt{\mu_0 \epsilon_0 \epsilon_{Gr} \left( 1 - \frac{j\sigma_{Gr}}{2\pi f \epsilon_0 \epsilon_{Gr}} \right)} \quad (21)$$

where  $\epsilon_0$  is permittivity of vacuum,  $\epsilon_{Gr}$  is relatively permittivity of substrate. Total reflection coefficient of the bilayer structure can be obtained by combining Equations (17) and (18):

$$\Gamma = \frac{E_0^-}{E_0^+} = \frac{(a_{01} + 1)\eta_m - (1 - a_{01})\eta_{air}}{(a_{01} + 1)\eta_m + (1 - a_{01})\eta_{air}} \quad (22)$$

To obtain Equation (22), magnetic field is related to electric field by intrinsic impedance as  $H = E/\eta$ . Here,  $\eta_{air} = 377 \Omega$ , intrinsic impedance for air, and  $\eta_m$ , intrinsic impedance for thin film, can be calculated by

$$\eta_m = (1 + j) \sqrt{\frac{\pi f \mu_0}{\sigma_{Cu}}} \quad (23)$$

Therefore,  $a_{01}$  in the Equation (22) can be expressed as follows:

$$a_{01} = \frac{\eta_s - \eta_m \exp(-2\gamma_m t_m)}{\eta_s + \eta_m} \quad (24)$$

And  $\eta_s = j2\pi f \mu_0 / \gamma_s$  is the intrinsic impedance for substrate.

Equations (22)–(24) indicate that the total reflection coefficient  $\Gamma$  depends on the electrical properties of the Cu coatings  $\sigma_{Cu}$  and substrate  $\sigma_{Gr}/\epsilon_{Gr}$ , as well as the thickness of the Cu film  $d_{Cu}$  and the operating frequency  $f$  [29,44].

The energy of the attenuated electromagnetic waves primarily dissipates in the form of power loss, which is a function of the effective conductivity of Cu/graphite. Therefore, the relationship between electromagnetic wave attenuation and power loss can be established through the effective conductivity of Cu/graphite. Similarly, when  $d_{Cu} \geq 3\delta_{Cu}$ , the electromagnetic waves are completely attenuated in the Cu coatings, and the total

reflection coefficient is only related to  $\sigma_{Cu}$ ,  $d_{Cu}$ , and  $f$ . On the basis of Figure 3, we can infer that, although the direct determination of the influence of rough surfaces, interfaces, and substrates on RF conductivity is challenging, a quantitative analysis can be achieved. The impact of rough surfaces, interfaces, and substrates on RF conductivity can be quantified by the correlation between effective conductivity and electromagnetic wave power loss. This entails comparing the power loss of a conductor with rough surfaces, interfaces, and substrates to that of a smooth conductor. Therefore, it is imperative to quantitatively calculate the electromagnetic wave power loss caused by rough surfaces, interfaces, and substrates.

Figure 4 illustrates the process of determining the ratio of power loss between the rough and dual layered conductors and smooth conductors. To simplify the problem, we initially consider the scenario where  $d_{Cu} \geq 3\delta_{Cu}$ , as depicted in Figure 4a. In this case, the effective conductivity of the rough conductor is solely affected by the presence of rough surfaces on the power loss. This effect can be determined by calculating the ratio of power loss between conductors with rough surfaces and smooth conductors. The known parameters include  $\sigma_{Cu}$ ,  $\delta_{Cu}$ ,  $d_{Cu}$ ,  $f$ , and the characteristic values of the rough surface, such as  $R_{rms}$  and  $R_s$ , which can be obtained through confocal microscopy. The loaded quality factor of the system  $Q_{load}$  can be obtained through separate resonant cavity testing. The effective conductivity  $\sigma'_{eff}$ , incorporating the rough surface, can be derived using Formulas (9)–(13). The losses in the system encompass not only those of the sample but also the losses of the cavity wall itself, denoted by  $P_{c1}$  and  $P_{c2}$ . Therefore, it is essential to independently quantify the additional power loss attributed to the rough surface ( $P'_{c3}$ ). Subsequently,  $P_{c1} + P_{c2} + P'_{c3} / P_{c1} + P_{c2} + P_{c3}$  can be calculated with Formulas (9)–(13). Combined with the inverse relationship between RF conductivity and power loss,  $\sigma_c / \sigma_{eff}$ , denoted by the introduced parameter  $\beta_{surface}$ , can be obtained. Furthermore, when  $d_{Cu} < 3\delta_{Cu}$ , as indicated in Figure 4b, the  $P'_{c3}$  of the rough surface can be determined. Additionally,  $\sigma_{eff}$  and  $\sigma_{Gr}$  can be obtained through separate resonant cavity testing. Using the theoretical formula for  $\sigma_{eff}$ , the conductivity of the Cu part contained in  $\sigma_{eff}$ , denoted as  $\sigma_{Cu}$ , and the interface conductivity  $\sigma_i$  can be determined [44]. Based on the theoretical relationship between conductivity and power loss, the power loss ratio of Cu/graphite and smooth pure Cu can be calculated. Similarly,  $\sigma'_c / \sigma_{eff}$  can be obtained, represented by the introduced parameter  $\beta$ , as illustrated in Figure 4b.

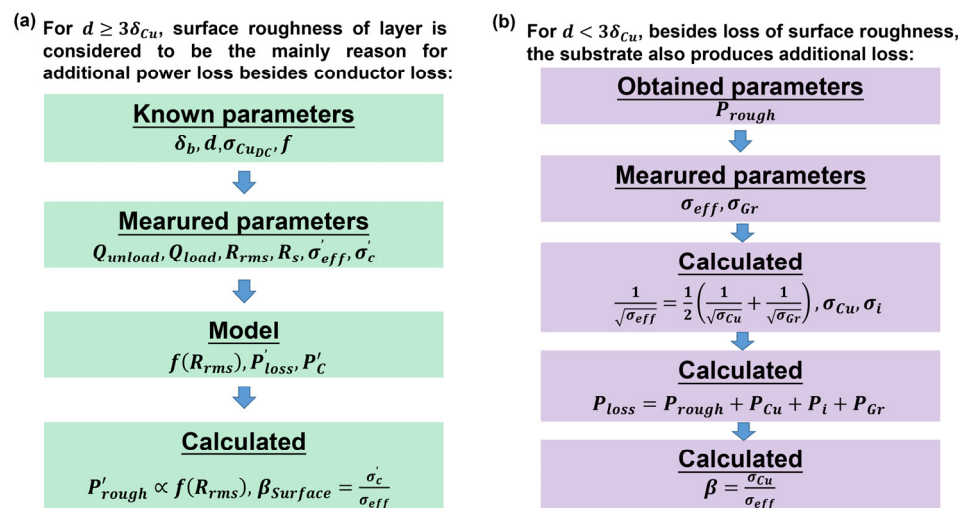


**Figure 4.** The derivation process of the influence of surface roughness, interface, and substrate on the effective conductivity of composite materials for cases  $d_{Cu} \geq 3\delta_{Cu}$  and  $d_{Cu} < 3\delta_{Cu}$ : (a) the derivation process of the influence of surface roughness on the effective conductivity of composite materials when  $d_{Cu} \geq 3\delta_{Cu}$ . (b) The derivation process of the influence of surface roughness, interface, and substrate on the effective conductivity of composite materials when  $d_{Cu} < 3\delta_{Cu}$ .

Following the theoretical calculation process depicted in Figure 4, our initial step is modeling surface roughness to calculate the additional  $P'_{c3}$ . This modeling approach enables us to quantitatively evaluate the impact of surface roughness on the RF conductivity of Cu/graphite. In contrast to many numerical models for roughness [40], this study employs fractal theory for modeling rough surfaces. Originally formulated by Mandelbrot, the fractal theory has evolved over the years and gained popularity among researchers due to its ability to more accurately describe surfaces that are neither periodic nor entirely random [45,46].

According to fractal theory, the function expression for the roughness model is provided as follows [47–49]:

$$Z(x) = G^{D-1} \sum_{n=n_1}^{\infty} \frac{\cos(2\pi\gamma^n x)}{\gamma^{(2-D)n}}, (1 < D < 2, \gamma > 1) \tag{25}$$

here,  $Z(x)$  represents the height of the random surface profile, and  $x$  signifies the position coordinates of the profile.  $D$  is the fractal dimension, and  $G$  is the characteristic scale parameter reflecting the amplitude magnitude and determining the specific size of  $Z(x)$ .  $\gamma^n$  represents the spatial frequency of the profile, where  $\gamma = 1.5$  is applicable to the randomness of high-frequency spectral density and phase for profiles that follow a normal distribution. Since the roughness profile is a non-stationary stochastic process, the relationship between the lowest frequency of the profile structure and the length of the roughness sample is provided by  $\gamma^{n_1} = 1/L_1$ , the initial term of the fractal function, which is an integer, and  $L_1$ , which is the sampling length of the roughness sample.

The derived power spectral density function is as follows:

$$\hat{P}(\omega) = \frac{G^{2(D-1)}}{2} \sum_{n=n_1}^{\infty} \frac{\delta(\omega - \gamma^n)}{\gamma^{(4-2D)n}} \tag{26}$$

$\delta$  is the radial function, defined as

$$\delta(x) = 0, (x \neq 0) \tag{27}$$

$$\int_{-\infty}^{\infty} \delta(x) dx = 1 \tag{28}$$

The continuous power spectrum can be approximated as

$$P(\omega) = \frac{G^{2(D-1)}}{2 \ln \gamma} \cdot \frac{1}{\omega^{(5-2D)}}, \gamma^{n_1} < \omega < \infty \tag{29}$$

It is evident that the continuous power spectrum  $P(\omega)$  enables a power law, which is fundamental to the fractal characterization of surface micro-topography. The fractal dimension  $D$  is linked to the extent of variation in the amplitude of the surface topography. A higher  $D$  value suggests the existence of more high-frequency components and richer details on the surface. The relationship between the parameters in the fractal method and the roughness parameters of the surface is as follows:

$$R_a < \frac{2G^{D-1}}{\pi} \frac{\gamma^{(D-2)n_1}}{1 - \gamma^{D-2}}, n_1 > 0 \tag{30}$$

the relationship between  $R_a$  and the amplitude coefficient  $G$  is  $R_a \propto G^{D-1}$ .

Generally, a smaller  $R_a$  corresponds to a larger fractal parameter  $D$ . Based on the established fractal model, the power loss of a semi-infinite planar waveguide is calculated. The variation range of the surface contour lines is taken from  $y = f(x)$  to  $y = -\infty$  on the three-dimensional model of the waveguide. The conductor is defined as a smooth plane when  $f(x) \equiv 0$ . Assuming that the varying magnetic field  $H_0 e^{j\omega t}$  propagates along

the surface  $f(x)$  in the Z direction, the eddy currents propagate in the  $x0y$  plane. The small changes in the magnetic field caused by finite conductors are negligible. Due to the small surface roughness induced by height variation, it is assumed that the magnetic field  $H_0$  remains unchanged due to variations in the  $y$  direction. The calculation of the eddy currents assumes no variation in  $H_0$  along the Z direction. Within the given volume  $V$  in the conductor, the eddy current losses are [40,50–52]

$$P = \frac{1}{2\sigma} \iiint_V J \times J^* dV = \frac{1}{2\sigma} \iiint_V (\nabla \times H) \cdot (\nabla \times H)^* dV \quad (31)$$

For conductors,  $\omega\epsilon/\sigma \ll 1$ . Therefore, the displacement current can be ignored. For the alternating magnetic field in the conductor, the equation is satisfied as follows:

$$\nabla^2 H = j\omega\mu\sigma H \quad (32)$$

where  $J = \nabla \times H$  is the conduction current density vector.

Since  $H$  only has a Z component, we have  $H = H_Z \hat{Z}$ , where  $\hat{Z}$  is the unit vector in the Z direction. Therefore, we obtain

$$\nabla \times H = \nabla \times H_Z \hat{Z} = \nabla H_Z \times \hat{Z} \quad (33)$$

$$\frac{\partial^2 H_Z}{\partial x^2} + \frac{\partial^2 H_Z}{\partial y^2} = \frac{j^2}{\delta_s^2} H_Z \quad (34)$$

Therefore,

$$\nabla^2 H_Z = \frac{j^2}{\delta_s^2} H_Z \quad (35)$$

where  $\hat{Z}$  is the unit vector in the Z direction, we obtain

$$P = \frac{1}{2\sigma} \iiint_V (\nabla H_Z) \cdot (\nabla H_Z^*) dV \quad (36)$$

Based on Green's formula, if there is any continuous differentiable function  $\psi, \phi$ , we obtain

$$\iiint_V (\nabla \psi) \cdot (\nabla \phi) dV = \iint_S \left( \psi \frac{\partial \phi}{\partial n} \right) \cdot dS - \iiint_V \psi (\nabla^2 \phi) dV \quad (37)$$

where  $S$  is the closed surface surrounding  $V$  and  $n$  is the outer normal direction of  $S$ .

Order  $\psi = H_Z, \phi = H_Z^*$ , we obtain

$$\iiint_V (\nabla H_Z) \cdot (\nabla H_Z^*) dV = \iint_S \left( H_Z \frac{\partial H_Z^*}{\partial n} \right) \cdot dS - \iiint_V H_Z (\nabla^2 H_Z^*) dV \quad (38)$$

Order  $\psi = H_Z^*, \phi = H_Z$ , we obtain

$$\iiint_V (\nabla H_Z^*) \cdot (\nabla H_Z) dV = \iint_S \left( H_Z^* \frac{\partial H_Z}{\partial n} \right) \cdot dS - \iiint_V H_Z^* (\nabla^2 H_Z) dV \quad (39)$$

Adding Equations (38) and (39) together provides

$$P = \frac{1}{2\sigma} \frac{1}{2} \left[ \iint_S \left( H_Z^* \frac{\partial H_Z}{\partial n} \right) + \left( H_Z \frac{\partial H_Z^*}{\partial n} \right) \cdot dS - \iiint_V H_Z^* (\nabla^2 H_Z) + H_Z (\nabla^2 H_Z^*) dV \right] \quad (40)$$

From  $\nabla^2 \mathbf{H} = j\omega\mu\sigma\mathbf{H}$ , the following can be obtained:

$$\nabla^2 H^* = -j\omega\mu\sigma H^* \tag{41}$$

Therefore,

$$H_Z^* (\nabla^2 H_Z) + H_Z (\nabla^2 H_Z^*) = 0 \tag{42}$$

We can obtain

$$P = \frac{1}{2\sigma} \frac{1}{2} \iint \left[ H_Z^* \frac{\partial H_Z}{\partial n} \right] + \left[ H_Z \frac{\partial H_Z^*}{\partial n} \right] dS \tag{43}$$

Taking a differential element  $dV$  of the conductor, with width  $z$  in the  $x$  direction and unit length  $\Delta x$  in the  $Z$  direction and extending infinitely deep in the  $y$  direction. Since  $\partial H_Z / \partial Z = 0$ , the surface integral at the  $Z$  terminal is 0; on the surfaces at  $x = x_0$  and  $x = x_0 + \Delta x$ , the integral results cancel each other out; as  $y$  approaches  $-\infty$ , the field tends to 0, so only a portion of the upper surface  $S_1$  remains in the integral over the closed surface  $S$ . At this point,  $H_Z = H_0$ , so we have

$$P = \frac{1}{2\sigma} \text{Re} \iint_{S_1} H_Z^* \frac{\partial H_Z}{\partial n} dS = \frac{1}{2\sigma} \text{Re} H_0^* \iint_{S_1} \frac{\partial H_Z}{\partial n} dS \tag{44}$$

Using Green's formula again, let  $\psi = H_Z$ ,  $\phi = 1$ , and  $\psi = 1$ ,  $\phi = H_Z$ , respectively. Based on the calculated results and Equations (41) and (42),

$$\iint_{S_1} \frac{\partial H_Z}{\partial n} dS = \iiint_V \nabla^2 H_Z dV \tag{45}$$

Substituting Equation (45) into Equation (44),

$$P = \frac{1}{2\sigma} \text{Re} H_0^* \iiint_V \nabla^2 H_Z dV \tag{46}$$

Substituting  $\nabla^2 H_Z = 2jH_Z / \delta_s^2$  into Equation (46),

$$P = \frac{1}{2\sigma} \text{Re} H_0^* \iiint_V \frac{2j^2}{\delta_s^2} H_Z dV \tag{47}$$

Because  $2j / \delta_s^2$  is a plural number, it can be separated from integration in Equation (47) as follows:

$$P = \frac{1}{\sigma \delta_s^2} \times j \text{Re} H_0^* \iiint_V H_Z dV \tag{48}$$

Based on the fundamental properties of complex numbers, namely

$$\text{Re}(jH_0^*) = -\text{Im}H_0^* \tag{49}$$

Therefore,

$$P = -\frac{1}{\sigma \delta_s^2} \text{Im}H_0^* \iiint_V H_Z dV \tag{50}$$

Because the volume integral is performed in three directions,  $x \in (x_0, x_0 + \Delta x)$ ,  $y \in (-\infty, f(x))$ , and  $z \in (0, 1)$ , we can transform the triple integral in  $V$  volume interval (Equation (50)) into a double integral in the  $x_0y$  plane.

Therefore,

$$P = -\frac{1}{\sigma \delta_s^2} \text{Im}H_0^* \int_{x_0}^{x_0 + \Delta x} \int_{-\infty}^{f(x)} H_Z dy dx \tag{51}$$

where  $P$  is the power dissipated in the infinitesimal conductor element  $dV$ .

If the conductor has a rough surface, according to the previously established fractal surface roughness model for determining the surface profile, i.e.,  $f(x) = Z(x)$ , the power dissipated in the infinitesimal conductor element is provided by

$$P = -\frac{1}{\sigma\delta_s^2} ImH_0^* \int_{x_0}^{x_0+\Delta x} \int_{-\infty}^{Z(x)} H_Z dy dx \tag{52}$$

If the conductor has a smooth surface, i.e.,  $f(x) \equiv 0$ , then  $P_0$  is the following:

$$P_0 = -\frac{H_0^2}{\sigma\delta_s^2} Im \int_{x_0}^{x_0+\Delta x} \int_{-\infty}^0 e^{-\frac{(1+j)|y|}{\delta_s}} dy dx = \frac{H_0^2}{2\sigma\delta_s} \tag{53}$$

Therefore,

$$\frac{P}{P_0} = \frac{-2}{H_0^2\delta_s\Delta x} ImH_0^* \int_{x_0}^{x_0+\Delta x} \int_{-\infty}^{f(x)} H_Z dy dx \tag{54}$$

It should be noted that, when deriving the formula for the power loss in a semi-infinite conducting plane, it is assumed that the varying magnetic field is denoted as  $H_0e^{j\omega t}$  and for the sake of simplification. It is considered that  $H_0$  does not vary with the  $x$  and  $z$  coordinates. However, in actual waveguide structures, the magnetic field on the conductor surface has three components:  $H_x$ ,  $H_y$ , and  $H_z$ , which do vary with the  $x$ ,  $y$ , and  $z$  coordinates. For the cylindrical resonant cavity in this work, the power loss of the resonant cavity has already been provided by Equations (9)–(11). Therefore, the difference in power loss between rough surface and smooth surface only lies in the loss  $P_{c3}$  on the  $S_3$  surface of the test metal plate. For the rough surface with a contour  $f(x)$ , the expression for  $P'_{c3}$  is

$$P'_{c3} = \frac{R_{s3}}{2} \int_{s3} |H_r(Z = f(x))|^2 ds \tag{55}$$

Therefore, for the cylindrical resonant cavity studied in this research, Equation (32) can be modified by defining  $\beta_{surface}$  as the ratio of power loss between rough and smooth surfaces as follows:

$$\beta_{surface} = \frac{P_{c1} + P_{c2} + P'_{c3}}{P_{c1} + P_{c2} + P_{c3}} \tag{56}$$

Based on Equations (6)–(13) and (33)–(35), it is possible to determine the specific values of  $\beta_{surface}$  at different frequencies.

According to the theoretical calculation process on the right side of Figure 4, it is first necessary to obtain  $\sigma_{Gr}$  and  $\sigma_i$  at different frequencies to calculate the specific values at different frequencies. The value of  $\sigma_{Gr}$  at different frequencies can be directly measured through the separated resonant cavity.  $\sigma_i$  has been obtained by numerous researchers through testing [18]. According to the work of Takashi Shimizu, the effective interfacial conductivity of the composite material can be provided by the following equation [53]:

$$\sigma_i = \frac{A}{\pi\mu_0 f_0^3 \sigma_0} \left[ \frac{1}{Q_u} - \frac{2}{f_0} (B\epsilon_r \tan\delta + C\epsilon_{rs} \tan\delta_s) \right]^{-2} \tag{57}$$

where  $A$ ,  $B$ , and  $C$  are represented as follows:

$$A = -\frac{\Delta f_{0t}^2}{\Delta_t} \tag{58}$$

$$B = -\frac{\Delta f_{\epsilon_r}}{\Delta_{\epsilon_r}} \tag{59}$$

$$C = -\frac{\Delta f_{\epsilon_{rs}}}{\Delta \epsilon_{rs}} \tag{60}$$

Whereas, due to the perturbations of  $t$ ,  $\epsilon_r$ , and  $\epsilon_{rs}$ , the variations in each resonance frequency  $\Delta f_{0t}$ ,  $\Delta f_{\epsilon_r}$ , and  $\Delta f_{\epsilon_{rs}}$  are calculated based on rigorous analysis using the mode matching method [53].

According to the derivation process shown in Figure 4, combined with Equations (36)–(39), the quantitative calculation is performed to evaluate the effects of surface roughness, interface, and substrate on the effective conductivity of composite materials under the condition of  $d_{Cu} < 3\delta_{Cu}$ . The ratio of power loss between the defined rough surface composite material and the smooth surface pure metal is defined as  $\beta$ . The value of  $\beta$  is provided by

$$\beta = P_{c1} + P_{c2} + P'_{c3} + P_i + P_{substrate} / P_{c1} + P_{c2} + P_{c3} \tag{61}$$

Based on Equations (56) and (61),  $\sigma_c / \beta$  and  $\sigma_c / \beta_{surface}$  are calculated at different frequencies, and the fitting curves of their variations with skin depth are plotted. The comparison with the measured values  $\sigma_{eff}$  is shown in Figure 5.

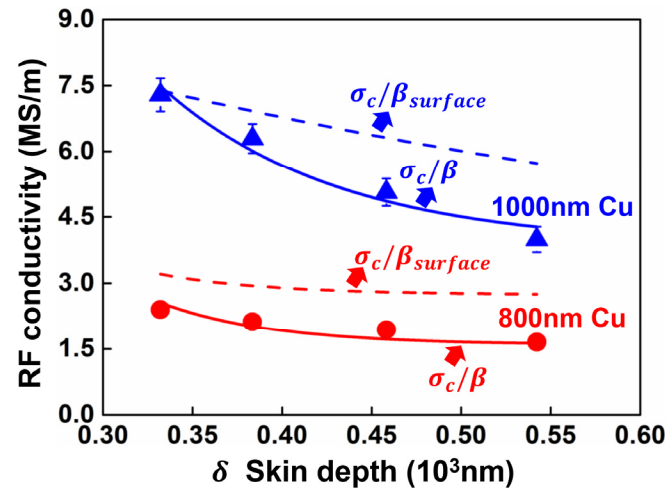


**Figure 5.** Comparison of fitted curves with measured results considering only surface roughness and considering the effects of surface roughness, interface, and substrate on the effective conductivity of Cu/graphite materials.

On the one hand, Figure 5 demonstrates the trend of the RF conductivity test values of the Cu/graphite samples with respect to the skin depth of Cu. The blue triangles represent the RF conductivity test values for the 1000 nm Cu/graphite and the red circles represent the RF conductivity test values for the 800 nm Cu/graphite. It can be found that the RF conductivity of the Cu/graphite gradually decreases as the Cu skin depth increases. This is mainly because the proportion of the graphite in the skin layer of the Cu/graphite gradually increases with increasing skin depth, resulting in a significant increase in the microwave power loss.

On the other hand, Figure 5 also displays the RF conductivity values of the Cu/graphite calculated by only considering the additional power loss of the surface roughness of the Cu film (denoted by  $\sigma_c / \beta_{surface}$ ), and the trends of  $\sigma_c / \beta_{surface}$  with the Cu skin depth are shown by the blue and red dashed lines, representing the cases of the 1000 nm Cu and 800 nm Cu, respectively. Correspondingly, the calculated value of the RF conductivity of the Cu/graphite when simultaneously considering the power loss from the surface roughness of the Cu film, the Cu/graphite interface, and the graphite substrate is denoted by  $\sigma_c / \beta$ . Similarly, the trend of  $\sigma_c / \beta$  with the Cu skin depth is denoted by the blue and red solid lines, representing the cases of 1000 nm Cu and 800 nm Cu, respectively. For the 1000 nm Cu, both the  $\sigma_c / \beta_{surface}$  and  $\sigma_c / \beta$  values differed little from the test at a Cu skin depth of about 330 nm. However, as the skin depth increases, the difference between the

value of  $\sigma_c/\beta_{surface}$  and the tested value gradually becomes larger. However, the value of  $\sigma_c/\beta$  is always less different from the tested value. This is due to the fact that the coating thickness of the 1000 nm Cu is greater than  $3\delta_{Cu}$ , which makes the electromagnetic wave completely attenuated in the Cu coatings when the skin depth of the Cu film is 330 nm. It can be seen from Figure 3c that the surface roughness of the Cu coatings is the main factor affecting the Cu/graphite RF conductivity, leading to the values of  $\sigma_c/\beta_{surface}$  and  $\sigma_c/\beta$  at this point being less different from the test values of the RF conductivity.

When the skin depth of Cu is greater than 330 nm, the electromagnetic waves in both the 1000 nm Cu/graphite and 800 nm Cu/graphite penetrate the Cu coatings and Cu/graphite interface, and finally are completely lost in the graphite substrate. Therefore, the loss of the electromagnetic wave is composed of the loss caused by the rough surface of the Cu coatings, the Cu/graphite interface, and the graphite substrate, as shown in Figure 3b. With the increase in the skin depth, the proportion of the graphite gradually increases, resulting in the proportion of the graphite loss gradually increasing. Therefore, the error of only considering the loss of the rough Cu coatings' surface gradually increases. With the increase in skin depth, the difference between the value of  $\sigma_c/\beta_{surface}$  and the test value gradually increases. Correspondingly, the difference between  $\sigma_c/\beta$  and the test value is always small. It indicates that, when the thickness of the Cu coatings is less than  $3\delta_{Cu}$ , it is more accurate to evaluate the RF conductivity of the Cu coatings by considering the losses caused by the rough surface of the Cu coatings, the Cu/graphite interface, and the graphite substrate.

Table 1 presents the differences between the fitting values of  $\sigma_c/\beta_{surface}$  and  $\sigma_c/\beta$  and the measured value  $\sigma_{eff}$  for the Cu skin depths corresponding to four frequency points between 15 and 40 GHz. For the 800 nm Cu/graphite, the difference between  $\sigma_c/\beta_{surface}$  and  $\sigma_{eff}$  (represented by  $|\Delta\sigma_1|/\sigma_M$  in Table 1) exceeds 30% and increases gradually with the increase in the skin depth, even exceeding 60%. For the 1000 nm Cu/graphite, the difference between  $\sigma_c/\beta_{surface}$  and  $\sigma_{eff}$  (represented by  $|\Delta\sigma_3|/\sigma_M$  in Table 1) is only 3.29% at  $\delta_{Cu} = 330$  nm, and it increases gradually with the increase in the skin depth, reaching a maximum of over 40%. The difference between the fitting value of  $\sigma_c/\beta$  and the measured value  $\sigma_{eff}$  is less than 7% (represented by  $|\Delta\sigma_2|/\sigma_M$  and  $|\Delta\sigma_4|/\sigma_M$  in Table 1), and it fluctuates only slightly with the variation in the skin depth.

**Table 1.** Considering only surface roughness and considering surface roughness ( $|\Delta\sigma_1|/\sigma_M$ ), interface, and substrate ( $|\Delta\sigma_2|/\sigma_M$ ) on the effective conductivity of Cu/graphite fitted curves versus measured values ( $\sigma_M$ ).

$\delta_{Cu}$ (nm)	800 nm Cu/Graphite			1000 nm Cu/Graphite		
	$\sigma_{eff}$ (MS/m)	$ \Delta\sigma_1 /\sigma_M$ (%)	$ \Delta\sigma_2 /\sigma_M$ (%)	$\sigma_{eff}$ (MS/m)	$ \Delta\sigma_3 /\sigma_M$ (%)	$ \Delta\sigma_4 /\sigma_M$ (%)
330	$2.40 \pm 0.078$	33.75	6.67	$7.29 \pm 0.378$	3.29	2.74
380	$2.12 \pm 0.074$	37.74	4.72	$6.29 \pm 0.333$	11.45	4.45
460	$1.94 \pm 0.068$	46.39	3.09	$5.06 \pm 0.311$	23.12	3.95
540	$1.65 \pm 0.065$	65.45	3.64	$3.99 \pm 0.288$	44.11	3.76

#### 4. Conclusions

In conclusion, we found that, when testing the radio frequency (RF) conductivity of copper/graphite using the split-resonator cavity technique, the measured values actually include the effective conductivity composed of copper (Cu) coatings with rough surfaces, the Cu/graphite interface, and the graphite substrate. By calculating the loss of the electromagnetic waves in the Cu/graphite and utilizing the inverse relationship between the microwave power loss and RF conductivity, the effective conductivity of Cu/graphite can be calculated. We compared the calculated RF conductivity of the Cu/graphite and measured RF conductivity of the Cu/graphite. The results show that the calculated effective conductivity of the Cu/graphite only considering the surface roughness factors has an error

generally higher than 30% compared to the measured results, while the error is less than 5% only in the region where  $d_{Cu} \geq 3\delta_{Cu}$ . When considering the power loss by the surface roughness of the Cu coatings, Cu/graphite interface, and graphite substrate, the error between the calculated and measured results of the RF conductivity of the Cu/graphite is generally less than 7% in both the  $d_{Cu} \geq 3\delta_{Cu}$  and  $d_{Cu} < 3\delta_{Cu}$  regions. Our study provides a reference for predicting the radio frequency conductivity of conductive coatings with a certain roughness in a specific skin depth range.

**Author Contributions:** Conceptualization, C.G. and Y.L.; formal analysis, C.G. and P.W.; investigation, C.G. and Y.L.; data curation, C.G.; writing—original draft preparation, C.G. and Y.L.; writing—review and editing, C.G., P.W., Y.L. and T.F.; supervision, Y.L. and T.F.; funding acquisition, T.F. All authors have read and agreed to the published version of the manuscript.

**Funding:** The authors acknowledge the financial support of Foundation of Science and Technology on High Power Microwave Laboratory, Grant HPM2209.

**Institutional Review Board Statement:** Not applicable.

**Informed Consent Statement:** Not applicable.

**Data Availability Statement:** Data are contained within the article.

**Conflicts of Interest:** The authors declare no conflict of interest.

## References

1. Wu, Z.C.; Chen, Z.H.; Du, X.; Logan, J.M.; Sippel, J.; Nikolou, M.; Katalin, K.; Reynolds, J.R.; Tanner, D.B.; Hebard, A.F.; et al. Transparent, conductive carbon nanotube films. *Science* **2004**, *305*, 1273–1276. [[CrossRef](#)] [[PubMed](#)]
2. Polosan, S.; Ciobotaru, I.C.; Ciobotaru, C.C. Organometallic coatings for electroluminescence applications. *Coatings* **2020**, *10*, 277. [[CrossRef](#)]
3. Islam, G.M.N.; Collie, S.; Gould, M.; Ali, M.A. Two-dimensional carbon material incorporated and PDMS-coated conductive textile yarns for strain sensing. *J. Coat. Technol. Res.* **2023**, *20*, 1881–1895. [[CrossRef](#)]
4. Pan, S.H.; Wang, T.L.; Jin, K.Y.; Cai, X.R. Understanding and designing metal matrix nanocomposites with high electrical conductivity: A review. *J. Mater. Sci.* **2022**, *57*, 6487–6523. [[CrossRef](#)]
5. Kim, S.; Jeong, H.; Choi, S.H.; Park, J.T. Electrical conductivity measurement of transparent conductive films based on carbon nanoparticles. *Coatings* **2019**, *9*, 499. [[CrossRef](#)]
6. Meng, F.; Huang, J. Fabrication of conformal array patch antenna using silver nanoink printing and flash light sintering. *AIP Adv.* **2018**, *8*, 085118. [[CrossRef](#)]
7. Yang, Y.F.; Yao, S.S.; Liu, Y.; Fan, T.X. Determining electrical conductivity of thin metal foils with micron-level thickness by an eddy current non-destructive method. *Nonferrous Met. Eng.* **2023**, *13*, 1–11.
8. Layani, T.M.E.; Daniel, K.; Tirosch, E.; Markovich, G.; Fleischer, S. Contact-free conductivity probing of metal nanowire films using THz reflection spectroscopy. *Nanotechnology* **2019**, *30*, 215702–215711. [[CrossRef](#)]
9. Mitta, S.B.; Choi, M.S.; Nipane, A.; Ali, F.; Kim, C.; Teherani, J.T.; Hone, J.; Yoo, W.J. Electrical characterization of 2D materials-based field-effect transistors. *2D Mater* **2021**, *8*, 012002. [[CrossRef](#)]
10. Moulzolf, S.C.; Frankel, D.J.; Lad, R.J. In situ four-point conductivity and Hall effect apparatus for vacuum and controlled atmosphere measurements of thin film materials. *Rev. Sci. Instrum.* **2002**, *73*, 2325–2330. [[CrossRef](#)]
11. Dasari, A.; Yu, Z.Z.; Mai, Y.W. Fundamental aspects and recent progress on wear/scratch damage in polymer nanocomposites. *Mat. Sci. Eng. R* **2009**, *63*, 31–80. [[CrossRef](#)]
12. Mizukami, K.; Watanabe, Y.; Ogi, K. Eddy current testing for estimation of anisotropic electrical conductivity of multidirectional carbon fiber reinforced plastic laminates. *Compos. Part A Appl. Sci. Manuf.* **2021**, *143*, 106274. [[CrossRef](#)]
13. Kang, J.H.; Kwang Min Yu, K.M.; Sang Hwa Lee, S.H.; Nahm, S.H.; Park, J.Y. Electrical conductivity evaluation techniques for superalloy single-crystal steel. *J. Electr. Eng. Technol.* **2023**, *18*, 1419–1427. [[CrossRef](#)]
14. Yu, Y.T.; Zhang, D.J.; Lai, C.; Tian, G.Y. Quantitative approach for thickness and conductivity measurement of monolayer coating by dual-frequency eddy current technique. *IEEE T. Instrum. Meas* **2017**, *66*, 1874–1882. [[CrossRef](#)]
15. Siang, T.W.; Firdaus Akbar, M.; Nihad Jawad, G.; Yee, T.S.; Mohd Sazali, M.I.S. A past, present, and prospective review on microwave nondestructive evaluation of composite coatings. *Coatings* **2021**, *11*, 913. [[CrossRef](#)]
16. Ma, W.H.; Li, C.W.; Wang, Z.Y.; Li, L.A.; Wang, S.B.; Sun, C.R. Application of terahertz time-domain spectroscopy in characterizing thin metal film-substrate structures. *IEEE Trans. Terahertz Sci. Technol.* **2020**, *10*, 593–598. [[CrossRef](#)]
17. Solemanifar, A.; Guo, X.; Donose, B.C.; Bertling, K.; Laycock, B.; Rakić, A.D. Probing peptide nanowire conductivity by THz nanoscopy. *Nanotechnology* **2022**, *33*, 065503. [[CrossRef](#)] [[PubMed](#)]

18. Tran, T.H.; She, Y.; Hirokawa, J.; Sakurai, K.; Kogami, Y.; Ando, M. Evaluation of effective conductivity of copper-clad dielectric laminate substrates in millimeter-wave bands using whispering gallery mode resonators. *Ieice Trans. Electron.* **2009**, *92*, 1504–1511. [[CrossRef](#)]
19. Kobayashi, Y.; Imai, T.; Kayano, H. Microwave measurement of temperature and current dependences of surface impedance for high-T<sub>c</sub> superconductors. *IEEE Trans. Microw. Theory Tech.* **1991**, *39*, 1530–1538. [[CrossRef](#)]
20. Xie, C.M.; Zhang, Y.P.; Niu, X.; Huang, M.; Gao, C.; Yu, C.Y.; Zheng, H.; Li, E. High-temperature measurement technology for microwave surface resistance of metal materials. *Int. J. RF Microw. Comput. Aided Eng.* **2023**, *2023*, 1–9. [[CrossRef](#)]
21. Li, Z.; Meng, Z.Z.; Wu, C.C.; Soutis, C.; Chen, Z.J.; Wang, P.; Gibson, A. A new microwave cavity resonator sensor for measuring coating thickness on carbon fibre composites. *NDT & E Int.* **2022**, *126*, 102584.
22. Nosov, R.N.; Sementsov, D.I. Skin effect under the conditions of ferromagnetic and spin-wave resonance. *Phys. Solid State* **2001**, *43*, 1923–1926. [[CrossRef](#)]
23. Ye, M.; Zhao, X.L.; Li, W.D.; Zhou, Y.; Chen, J.Y.; He, Y.N. Conductivity extraction using a 180 GHz quasi-optical resonator for conductive thin film deposited on conductive substrate. *Materials* **2020**, *13*, 5260. [[CrossRef](#)] [[PubMed](#)]
24. Morgan, S.P. Effect of surface roughness on eddy current losses at microwave frequencies. *J. Appl. Phys.* **1949**, *20*, 352–362. [[CrossRef](#)]
25. Nakayama, A.; Terashi, Y.; Uchimura, H.; Fukuura, A. Conductivity measurements at the interface between the sintered conductor and dielectric substrate at microwave frequencies. *IEEE Trans. Microw. Theory Tech.* **2002**, *50*, 1665–1674. [[CrossRef](#)]
26. Deng, H.W.; Zhao, Y.J.; Liang, C.J.; Jiang, W.S.; Ning, Y.M. Effective skin depth for multilayer coated conductor. *Prog Electromagn. Res.* **2009**, *9*, 1–8. [[CrossRef](#)]
27. Zhang, M.; Liu, J.; Liao, L.; Gao, H.; Zhu, D.B.; Zhuo, F.F.; Qi, P.S. A calculation method on high-frequency loss of double-layer composite conductor. *IEEE Trans. Electromagn. Compat.* **2017**, *60*, 647–656. [[CrossRef](#)]
28. Aizawa, Y.; Nakayama, H.; Kubomura, K.; Nakamura, R.; Tanaka, H. Theoretical study on lowering loss of skin effect suppressed multi-layer transmission line with positive/negative (Cu/NiFe) permeability materials for high data-rate and low delay-time I/O interface board. *AIP Adv.* **2020**, *10*, 015124. [[CrossRef](#)]
29. Collin, R.E. *Foundations for Microwave Engineering*, 2nd ed.; Wiley IEEE Press: New York, NY, USA, 2000; pp. 96–110.
30. Sasaki, K.; Katagiri, T.; Yusa, N.; Hashizume, H. Experimental verification of long-range microwave pipe inspection using straight pipes with lengths of 19–26.5m. *NDT & E Int.* **2018**, *96*, 47–57.
31. Taber, R.C. A parallel plate resonator technique for microwave loss measurements on superconductors. *Rev. Sci. Instrum.* **1990**, *61*, 2200–2206. [[CrossRef](#)]
32. Mazierska, J. Dielectric resonator as a possible standard for characterization of high temperature superconducting films for microwave applications. *J. Supercond.* **1997**, *10*, 73–84. [[CrossRef](#)]
33. Krupka, J. Measurements of the surface resistance and the effective conductivity of copper clad laminates employing dielectric resonator technique. *IEEE* **2007**, *1–6*, 515–518.
34. Kundu, S.K.; Karmakar, S.; Taki, G.S. Crystallinity study of Cu thin film deposited by indigenously developed DC magnetron sputtering setup. *Macromol. Symp.* **2023**, *407*, 2100356. [[CrossRef](#)]
35. Pierson, J.F.; Wiederkehr, D.; Billard, A. Reactive magnetron sputtering of copper, silver, and gold. *Thin Solid Films* **2005**, *478*, 196–205. [[CrossRef](#)]
36. Sato, N.; Endo, Y.; Yamaguchi, M. Skin effect suppression for Cu/CoZrNb multilayered inductor. *J. Appl. Phys.* **2012**, *111*, 07A501. [[CrossRef](#)]
37. Wu, Z.; Davis, L.E. Surface roughness effect on surface impedance of superconductors. *J. Appl. Phys.* **1994**, *76*, 3669–3672. [[CrossRef](#)]
38. Ding, R.H.; Tsang, L.; Braunisch, H. Wave Propagation in a Randomly Rough Parallel-Plate Waveguide. *IEEE Trans. Microw. Theory Tech.* **2009**, *57*, 1216–1223. [[CrossRef](#)]
39. Matsushima, A.; Nakata, K. Power loss and local surface impedance associated with conducting rough interfaces. *Electr. Commun. Jpn.* **2010**, *89*, 1–10. [[CrossRef](#)]
40. Tsang, L.; Braunisch, H.; Ding, R.H.; Gu, X.X. Random rough surface effects on wave propagation in interconnects. *IEEE Trans. Adv. Pack.* **2010**, *33*, 839–856. [[CrossRef](#)]
41. Jakubiuk, K.; Zimny, P. Skin effect in rectangular conductors. *J. Phys. A Math. Gen.* **1976**, *9*, 669–678. [[CrossRef](#)]
42. Weeks, W.T.; Wu, L.L.; Mcallister, M.F.; Singh, A. Resistive and inductive skin effect in rectangular conductors. *IBM J. Res. Develop.* **1979**, *23*, 652–660. [[CrossRef](#)]
43. Cao, B.H.; Li, C.; Fan, M.B.; Ye, B.; Gao, S. Analytical modelling of eddy current response from driver pick-up coils on multi-layered conducting plates. *Insight* **2018**, *60*, 77–83. [[CrossRef](#)]
44. Hirayama, N.; Nakayama, A.; Yoshikawa, H.; Shimizu, T.; Kogami, Y. Measurement technique for interface and surface conductivities at millimeter-wave frequencies using dielectric rod resonator excited by nonradiative dielectric waveguide. *IEEE Trans. Microw. Theory Tech.* **2022**, *70*, 2750–2761. [[CrossRef](#)]
45. Zou, M.Q.; Yu, B.M.; Feng, Y.J.; Xu, P. A Monte Carlo method for simulating fractal surfaces. *Phys. A* **2007**, *386*, 176–186. [[CrossRef](#)]
46. Majumdar, A.A.; Bhushan, B. Role of fractal geometry in roughness characterization and contact mechanics of surfaces. *J. Tribol.* **1990**, *112*, 205–216. [[CrossRef](#)]
47. Majumder, A.; Tien, C.L. Fractal characterization and simulation of rough surface. *Wear* **1990**, *136*, 313–327. [[CrossRef](#)]

48. Jordan, D.L.; Hollins, R.C.; Jakeman, E. Measurement and characterization of multiscale surfaces. *Wear* **1986**, *109*, 127–134. [[CrossRef](#)]
49. Li, N.; Zheng, F. Effect of micro/nano-scale rough surface on power dissipation of the waveguide: Model and simulate. *J. Nanosci. Nanotechnol.* **2011**, *11*, 11222–11226. [[CrossRef](#)]
50. Huang, B.; Jia, Q. Accurate modeling of conductor rough surfaces in waveguide devices. *Electronics* **2019**, *8*, 269. [[CrossRef](#)]
51. Tsang, L.; Gu, X.; Braunsch, H. Effects of random rough surface on absorption by conductors at microwave frequencies. *IEEE Microw. Wirel. Compon. Lett.* **2006**, *16*, 221–223. [[CrossRef](#)]
52. Li, N.; Duan, B.Y.; Zheng, F. Effect of the random error on the radiation characteristic of the reflector antenna based on two dimensional fractal. *Int. J. Antenn. Propag.* **2012**, *2012*, 1–6. [[CrossRef](#)]
53. Shimizu, T.; Hirano, Y.; Kogami, Y. Frequency dependence measurement technique of the interface conductivity using a dielectric rod resonator sandwiched between copper-clad dielectric substrates. In Proceedings of the 91st ARFTG Microwave Measurement Conference, Philadelphia, PA, USA, 15 June 2018; IEEE: Piscataway, NJ, USA, 2018.

**Disclaimer/Publisher’s Note:** The statements, opinions and data contained in all publications are solely those of the individual author(s) and contributor(s) and not of MDPI and/or the editor(s). MDPI and/or the editor(s) disclaim responsibility for any injury to people or property resulting from any ideas, methods, instructions or products referred to in the content.